Stiffness of the human foot and evolution of the transverse arch

Madhusudhan Venkadesan*[1], Ali Yawar[1], Carolyn M. Eng†[1], Marcelo A. Dias†[2,3,4], Dhiraj K. Singh‡[5], Steven M. Tommasini[6], Andrew H. Haims[6,7], Mahesh M. Bandi§[5], and Shreyas Mandre¶[8]

[1]*Department of Mechanical Engineering & Materials Science, Yale University, New Haven, CT 06520, USA*
[2]*School of Science, Aalto University, Espoo, FI-02150, Finland*
[3]*Nordic Institute for Theoretical Physics (NORDITA), Roslagstullsbacken 23, SE-106 91 Stockholm, Sweden*
[4]*Department of Engineering, Aarhus University, Inge Lehmanns Gade 10, 8000 Aarhus C, Denmark*
[5]*Nonlinear and Non-equilibrium Physics Unit, OIST Graduate University, 1919-1 Tancha, Onna-son, Okinawa 904-0495, Japan*
[6]*Department of Orthopaedics and Rehabilitation, Yale University, New Haven, CT 06520, USA*
[7]*Department of Radiology and Biomedical Imaging, Yale University, New Haven, CT 06520, USA*
[8]*Mathematics Institute, University of Warwick, Coventry CV4 7AL UK*

Abstract

The stiff human foot enables an efficient push-off when walking or running and was critical for the evolution of bipedalism.[1–6] The uniquely arched morphology of the human midfoot is thought to stiffen it,[5–9] whereas other primates have flat feet that bend severely in the midfoot.[7,10,11] However, the relationship between midfoot geometry and stiffness remains vigorously debated in foot biomechanics,[12,13] podiatry,[14,15] and palaeontology.[4–6] These ongoing debates centre on the medial longitudinal arch (MLA)[5,6] and have not considered whether stiffness is affected by the human foot's second, transverse tarsal arch (TTA).[16] Here we show that the TTA is responsible for over 40% of the foot's longitudinal stiffness. The underlying mechanical principle resembles a floppy currency note that stiffens significantly upon curling it along the transverse direction. We derive a dimensionless curvature parameter that governs the TTA's stiffness contribution, demonstrate its predictive power using mechanical mimics of the foot, and find its skeletal correlate in hominin feet. By analysing fossils, we track the evolution of the curvature parameter among extinct hominins and show that a human-like transverse arch was a key step in the evolution of human bipedalism that predates the genus *Homo* by at least 1.5 million years. This renewed understanding of the form and function of the foot may improve the clinical treatment of flatfoot disorders, the design of robotic feet, and the study of foot function in locomotion.

*mv@classicalmechanic.net
†Equal contribution
‡Present address: Engineering Mechanics Unit, Jawaharlal Nehru Centre for Advanced Scientific Research, Jakkur, Bangalore, 560064, India.
§bandi@oist.jp
¶shreyas_mandre@brown.edu

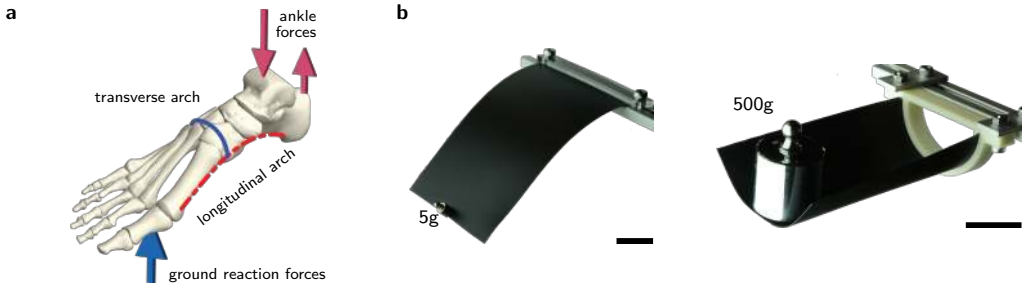

Figure 1. Transverse curvature in human feet and its effect on stiffness. a, The human foot has two distinct arches in the midfoot, the medial longitudinal arch (MLA) and the transverse tarsal arch (TTA). See Fig. E1 as an additional illustrated anatomical guide. The typical loading pattern during push-off in walking and running is shown here. **b,** A thin and floppy sheet of paper becomes significantly stiffer because of transversal curvature. The TTA may play a similar role in feet. Scale bars: 5 cm.

In walking and running, people apply large forces that exceed body weight when pushing-off with the ball of the foot.[17] Because of these forces, the midfoot experiences high sagittal-plane torques that bend the foot. A stiff midfoot therefore helps to efficiently utilize the mechanical power generated by the ankle during push-off, without absorbing the propulsive work as deformation of the foot.[2–4]

The unique longitudinal arch of the human midfoot is thought to underlie the greater stiffness of human feet compared to other primate feet (Table E1).[5,6,9,18] But stiffness is not a static quantity and muscle activity has been shown to dynamically modulate midfoot stiffness in both humans and apes.[13,19,20] Nevertheless, the static stiffness of the foot's structure forms the baseline around which the dynamic modulation occurs. Muscles with similar mechanical action to tissues responsible for static stiffness are likely to be important in stiffness modulation. Therefore, understanding the morphological underpinning of static stiffness is crucial for both static and dynamic conditions (Supplement S1.1–S1.3).

The human midfoot has two pronounced arches: the medial longitudinal arch (MLA) and a second, transverse tarsal arch (TTA) (Fig. 1a). Of these two arches, the MLA is extensively studied.[5,6,20] The MLA stiffens the midfoot partly through a bow-string arrangement with the stiff longitudinal fibres of the plantar fascia[7,9] and a windlass-like mechanism due to toe dorsiflexion just before push-off.[8,21] Besides the plantar fascia, the longitudinally oriented long plantar, short plantar and calcaneonavicular ligaments form a large fraction of the static midfoot stiffness in humans and other primates.[9,18] However, unlike the plantar fascia, the contribution of these ligaments is not affected by the height of the MLA, as seen from their nearly equal relative contributions to both arched human feet[9] and flat monkey feet (Table E1, Supplement S1.4).[18]

Despite these stiffness measurements in human and monkey feet, the relationship between the MLA height or curvature and midfoot stiffness remains controversial.[5,20] Some humans face no difficulty in

walking with a heel-to-toe style despite having little to no MLA.[12] Conflicting evidence in correlating MLA height with foot flexibility in foot disabilities[11,22] and from surgical reconstruction of the MLA[15] cast further doubt upon the relationship between the MLA and midfoot stiffness. There are also debates over when stiff midfeet arose in human evolution,[5,6] including what kind of foot made the 3.66 million-year-old, partly human-like footprints at Laetoli.[23,24]

These debates on arch morphology and stiffness centre around the MLA, plantar fascia, and other longitudinally oriented ligaments and muscles. The very definition of flatfoot relies mostly upon the height of the MLA.[12,22] However, the role of the second, transverse tarsal arch (TTA, Fig. 1a) in stiffening the midfoot remains unknown (Supplement S1.4). Just as slightly curling a thin sheet of paper in the transverse direction stiffens it longitudinally, the TTA may also stiffen the midfoot (Fig. 1b). To investigate whether the TTA functions in this manner, we performed three-point bending tests on arched continuum shells, mechanical mimics of the midfoot, and human cadaveric feet (see Methods).

To study the effect of the TTA, we modelled the midfoot as curved elastic shells in computer simulations and physical experiments (Fig. 2a). We found that shells with greater transverse curvature are stiffer in longitudinal bending (Fig. 2b inset). However, stiffness is also affected by the Young's modulus and Poisson's ratio of the material, and the thickness t, length L and width w. To isolate the contribution of the transverse arch to midfoot stiffness, we used scaling analysis to derive dimensionless stiffness and curvature variables that normalize for material property and size differences (Supplement S2). The normalized stiffness $\hat{K}$ is the ratio of the stiffness of the curved shell to that of a flat plate that is identical in all regards but for the curvature. The normalized curvature $\hat{c}$ encapsulates the mechanical coupling between bending out-of-plane and stretching in-plane that is induced by the transverse curvature c, and is given by,

$$\hat{c} = \frac{cL^2}{t}. \tag{1}$$

Collapse of the normalized data onto a master curve shows that $\hat{c}$ is the chief explanatory variable for $\hat{K}$ (Fig. 2b). There is a transition between two regimes around $\hat{c}_{\mathrm{tr}} = 10$. Stiffness $\hat{K}$ increases nonlinearly with curvature when $\hat{c} > \hat{c}_{\mathrm{tr}}$ but is mostly insensitive to curvature with $\hat{K} \approx 1$ when $\hat{c} < \hat{c}_{\mathrm{tr}}$. Increasing longitudinal curvature has no effect on stiffness (stars in Fig. 2b), because these shells lack any analogue of the plantar fascia. Transverse curvature stiffens the shell because out-of-plane longitudinal bending induces in-plane stretching of the shell's material in the transverse and all other directions close to the load application point (Fig. E2, Supplement S2). Therefore, transverse curvature has the effect of amplifying the intrinsic stiffness of a flat plate, whereas the longitudinal curvature has no similar effect.

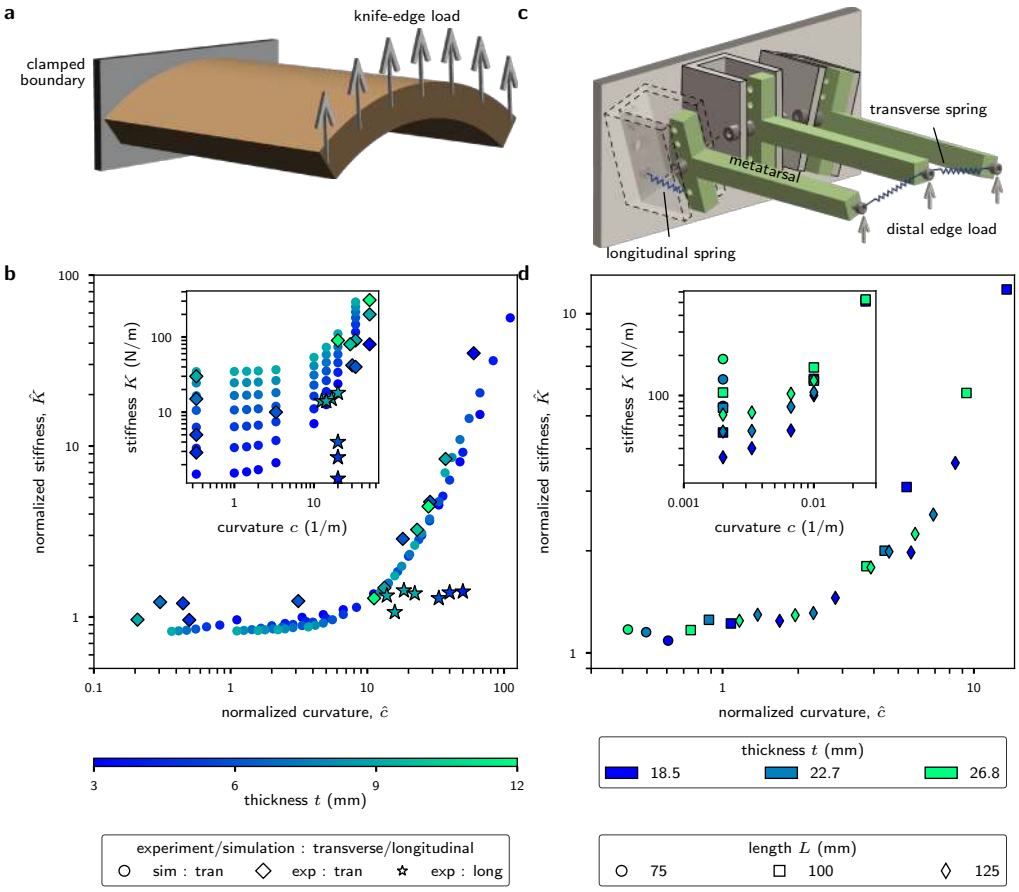

Figure 2. Curvature-induced stiffness in mechanical models of hominin feet. a, Continuum elastic shells with curvature were subjected to a distributed vertical load at one end and clamped at the other. **b, inset,** Stiffness K versus curvature c for continuum shells of various thickness t (blue shading) in experiments (diamonds and stars) and simulations (circles). **b,** Normalized stiffness $\hat{K}$ versus normalized curvature $\hat{c}$ for the same continuum shells as the inset. Experimental data include shells with just transverse curvature (diamonds) or longitudinal curvature (stars). **c,** Schematic of a discrete foot-mimic comprised of three metatarsals arranged in a transverse arch and loaded at the distal end. Longitudinal springs at the hinged base mimic the longitudinal ligaments in feet. Transversal inter-metatarsal springs at the distal end mimic transverse elastic tissues. **d, inset,** Stiffness K versus transverse curvature c for mimics of various lengths L and thickness t. **d,** The foot-mimic data visualized as normalized stiffness $\hat{K}$ versus normalized curvature $\hat{c}$. Close-up views of the continuum and discrete experiments are shown in Fig. E3 and E4, respectively.

We performed three-point bending tests on discrete mechanical mimics of the foot with a TTA and found similar results to the continuum shells (Fig. 2c,d). The mimics are comprised of three metatarsals with hinges towards the midfoot, and they varied in the length L, thickness t and transverse curvature c (Online Methods, Supplement S4). The longitudinal springs at the hinges mimic the longitudinal midfoot ligaments that contribute to midfoot stiffness whether arched or not (Supplement S1.4). The distally located transverse springs mimic inter-metatarsal tissues that influence the predicted bending-stretching coupling due to the transverse curvature. The measured stiffness of each mimic was normalized by that of a flat mimic, with dimensions similar to the foot of a chimpanzee, to yield the normalized stiffness $\hat{K}$

(equation M1). We find that the normalized curvature $\hat{c}$ accurately predicts the normalized stiffness $\hat{K}$ for discrete foot-like structures, as for continuum shells (Fig. 2d). The transition in stiffness from nearly curvature-insensitive to a nonlinear increase occurs around $\hat{c}_{\mathrm{tr}} = 3$ for the mimics. Although this value is different from continuum shells, bending-stretching coupling is the common mechanism for curvature-induced stiffness in continuum and discrete structures, and $\hat{c}$ emerges as the chief explanatory variable for that mechanism.

The curvature versus stiffness curve is unknown for human feet but we may test whether its $\hat{c}$ belongs to the curvature-induced stiffening regime by measuring the decrease in stiffness upon flattening the transverse arch. However, the TTA in a human foot cannot be selectively altered without affecting other aspects of the foot such as the MLA. So we designed a method to mimic flattening of the TTA without altering the skeletal structure. Analyses of the continuum shells and mechanical feet suggest that the TTA induces stiffness by coupling longitudinal bending with stretching of the inter-metatarsal tissues. Therefore, cutting the inter-metatarsal tissues should disrupt the stiffening mechanism and achieve the effect of flattening the arch without altering the skeletal arch. We tested this idea in the foot mimics by comparing the stiffness of transversally curved mimics that lack the inter-metatarsal springs against flat mimics with all springs intact. Both had the same stiffness (Fig. E5, $R^2 = 0.98$, slope=1.05, intercept = 0), showing that cutting the transverse springs is analogous to flattening the arch even though the cuts did not alter the arch curvature.

To determine the TTA's contribution to stiffness in human feet, we performed three-point bending tests on two human cadaveric feet (Fig. 3a, Online methods, Supplement S5.2) and assessed the effect of selectively cutting the transverse elastic tissues between the metatarsals (T^- condition, Fig. 3b, Fig. E1b). To carefully preserve longitudinal elastic tissues, the cuts were restricted to the transverse metatarsal ligaments, the skin between the toes and the inter-metatarsal tissues near the dorsal surface of the foot. Cutting these transverse tissues caused a decline in stiffness of 44% and 54% for the two feet (Fig. 3b, Table E1). Each foot serves as its own control, thereby quantifying the TTA's contribution in terms of the normalized stiffness $\hat{K} = K_{\mathrm{intact}}/K_{\mathrm{T}^-}$, i.e. $\hat{K} = 1.79$ and 2.17 for the feet whose $\hat{c} = 15.4$ and 16.0, respectively (Fig. 4b, equation M4).

The cadaveric experiments show that the inter-metatarsal tissues contribute substantially to foot stiffness and more than the previously known 30% contribution of the MLA and plantar fascia (Table E1, Supplement S1.4). The mechanistic understanding of transversally curved structures implies that the inter-metatarsal tissues affect the longitudinal bending stiffness of the foot because the human TTA with $\hat{c} \approx 15$ is sufficiently arched to couple longitudinal bending and transverse stretching. Unlike the plantar

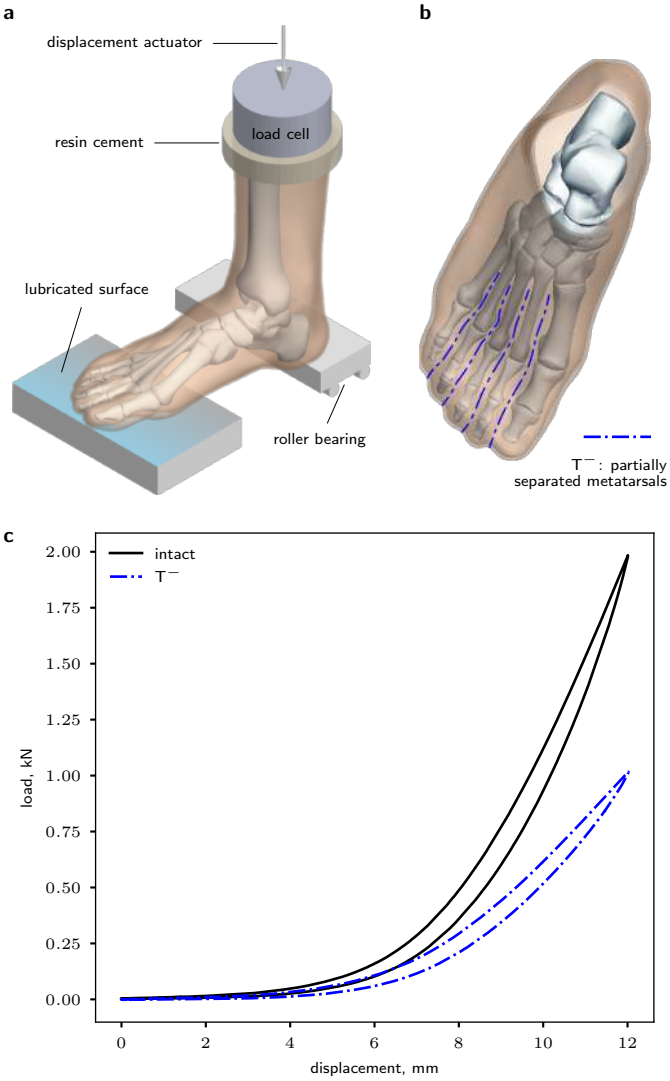

Figure 3. Three-point bending test on a cadaveric human foot. a, Fresh-frozen cadaveric feet were thawed and mounted in a materials testing machine via an attachment at the transected shank. The distal end of the heel rested on a sliding platform with low-friction roller bearings to allow changes to the foot length. The ball of the foot and the toes rested on a highly lubricated surface to allow all natural deformations. A known displacement was applied at the transected shank and the reaction force measured to quantify the foot's stiffness. Tests were performed on intact feet and those with transversal cuts (T^-). **b,** The transversal cuts between the toes and metatarsals were no deeper than the plantar plane of the metatarsal shafts (T^-: blue lines). **c,** Displacement versus load traces for an intact (black, solid line) and a T^- (blue, dashed line) foot. Some stress relaxation was observed during the initial few cycles of testing and the last cycle was used in analyses.

fascia and the inter-metatarsal tissues, the long plantar, short plantar and calcaneonavicular ligaments form part of the intrinsic stiffness of the midfoot that are not affected by either the MLA or TTA curvatures (Supplement S1.4). However, additional work is needed to discover the curvature-stiffness curve that apply to human feet. Furthermore, the stiffness contributions from the two arches may not simply add during *in vivo* foot function and further work is needed to investigate interactions between the arches.

We use $\hat{c}$ to compare the TTA among hominins and track its evolution (Fig. 4, see also Supple-

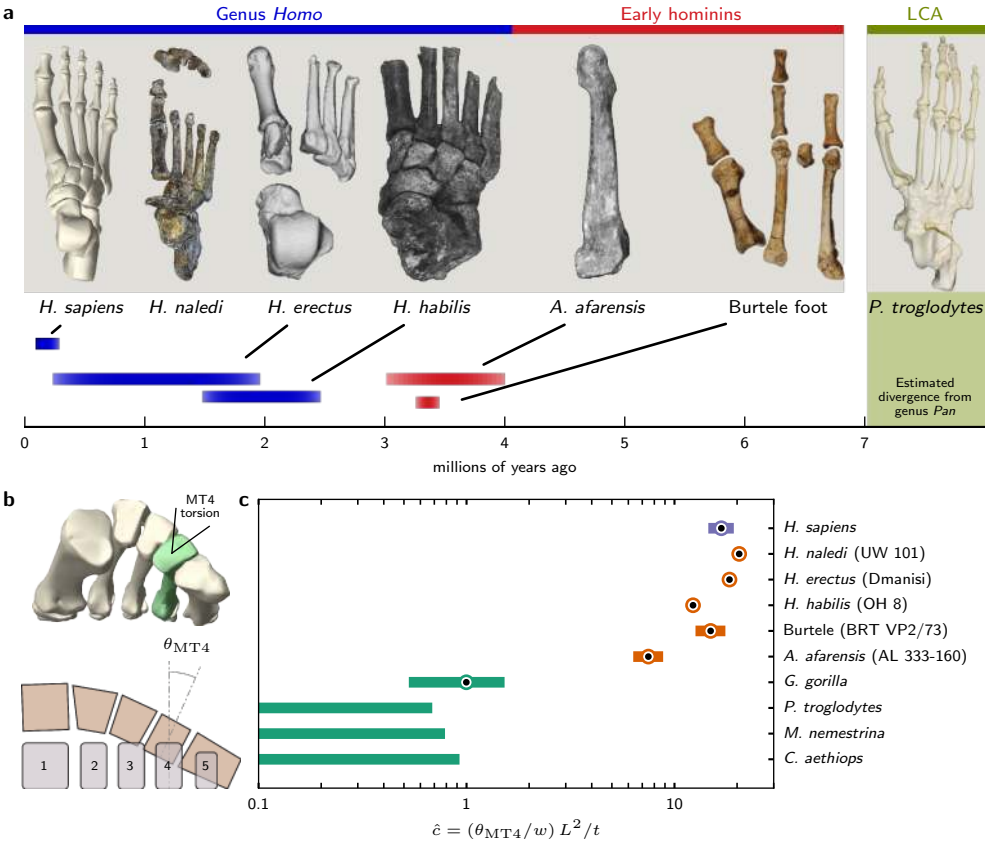

Figure 4. Transverse curvature of extant and extinct feet. a, Representative images of feet used in our analyses and their respective estimated survival dates: *H. naledi*,[25] *H. erectus*,[26] *H. habilis*,[27], *A. Afarensis*,[28] Burtele.[29] *Pan troglodytes* represents the last common ancestor (LCA) of humans and chimpanzees. **b,** Schematics showing the skeletal view of the TTA and the torsion of the fourth metatarsal induced by the mediolateral packing of the tarso-metatarsal bones. **c,** Median (dot with circle) and the middle 50th percentile (shaded bar) of the normalized curvature $\hat{c}$ are shown on a logarithmic scale. Tables E2 and E3 summarize the morphometric data used in estimating $\hat{c}$.

ment S5). At one extreme are the vervet monkey, macaque, chimpanzee and gorilla feet, all of which have $\hat{c} < 2$, substantially flatter than humans whose $\hat{c} > 10$. At the other extreme are species in the genus *Homo*, including *Homo naledi*,[25] *Homo habilis*,[27], and *Homo erectus*[26] that have a pronounced TTA whose $\hat{c}$ falls within the normal human range around $\hat{c} \approx 15$. Surprisingly, the estimated $\hat{c}$ of the approximately 3.4 million year-old Burtele foot (from an unidentified species) falls within normal human variation despite having an abducted hallux.[29] In contrast, the estimated $\hat{c}$ of an approximately 3.2 million year-old *Australopithecus afarensis* (AL-333) falls below the human range, despite a human-like degree of torsion of the fourth metatarsal.[28]

Additional data are needed, especially from earlier hominins like *Ardipithecus*, but the available evidence suggests several stages in the evolution of the arch of the human foot.[5,6] First, apes like chimpanzees and presumably the last common ancestor of apes and hominins lack both a MLA and a TTA, and thus are able to stiffen the midfoot only partially using muscles.[5] By 3.4 million years ago, possibly

earlier, a human-like TTA had evolved that may have increased midfoot stiffness during propulsion in the Burtele hominin (Supplement S5.4). Compared to humans, the TTA was apparently less developed in *A. afarensis*, which also lacked a fully developed MLA,[28] consistent with analyses of the 3.66 million year-old Laetoli G footprints thought to have been made by *A. afarensis*.[24,30] Finally, in the genus *Homo* we see a full MLA and TTA, enabling both effective walking and running. These inferences need to be tested with additional fossils incorporating not just analyses of the MLA but also the TTA.

Our findings show a new and substantial functional role for the TTA in midfoot stiffness. Traditional thinking in biomechanics, human evolution and current clinical practice with an emphasis on the sagittal plane and the MLA should thus be expanded to incorporate the TTA and the transverse axis that is orthogonal to the sagittal plane.

References

[1] Susman, R. L. Evolution of the Human Foot: Evidence from Plio-Pleistocene Hominids. *Foot & Ankle International* **3**, 365–376 (1983).

[2] Bramble, D. M. & Lieberman, D. E. Endurance running and the evolution of Homo. *Nature* **432**, 345–352 (2004).

[3] Takahashi, K. Z., Gross, M. T., Van Werkhoven, H., Piazza, S. J. & Sawicki, G. S. Adding stiffness to the foot modulates soleus force-velocity behaviour during human walking. *Scientific reports* **6**, 29870 (2016).

[4] Pontzer, H. Economy and endurance in human evolution. *Current Biology* **27**, R613–R621 (2017).

[5] Holowka, N. B. & Lieberman, D. E. Rethinking the evolution of the human foot: Insights from experimental research. *Journal of Experimental Biology* **221**, jeb174425 (2018).

[6] DeSilva, J., McNutt, E., Benoit, J. & Zipfel, B. One small step: A review of plio-pleistocene hominin foot evolution. *American journal of physical anthropology* **168**, 63–140 (2019).

[7] Morton, D. J. Evolution of the longitudinal arch of the human foot. *Journal of Bone and Joint Surgery* **6**, 56–90 (1924).

[8] Hicks, J. H. The mechanics of the foot: II. The plantar aponeurosis and the arch. *Journal of Anatomy* **88**, 25–& (1954).

[9] Ker, R. F., Bennett, M. B., Bibby, S. R., Kester, R. C. & Alexander, R. M. The spring in the arch of the human foot. *Nature* **325**, 147–149 (1987).

[10] D'Août, K., Aerts, P., De Clercq, D., De Meester, K. & Van Elsacker, L. Segment and joint angles of hind limb during bipedal and quadrupedal walking of the bonobo (pan paniscus). *American Journal of Physical Anthropology* **119**, 37–51 (2002).

[11] Bates, K. T. *et al.* The evolution of compliance in the human lateral mid-foot. *Proceedings of the Royal Society B: Biological Sciences* **280**, 20131818–20131818 (2013).

[12] DeSilva, J. M. *et al.* Midtarsal break variation in modern humans: Functional causes, skeletal correlates, and paleontological implications. *American Journal of Physical Anthropology* **156**, 543–552 (2015).

[13] Holowka, N. B., O'Neill, M. C., Thompson, N. E. & Demes, B. Chimpanzee and human midfoot motion during bipedal walking and the evolution of the longitudinal arch of the foot. *Journal of Human Evolution* **104**, 23–31 (2017).

[14] MacKenzie, A. J., Rome, K. & Evans, A. M. The efficacy of nonsurgical interventions for pediatric flexible flat foot: a critical review. *Journal of Pediatric Orthopaedics* **32**, 830–834 (2012).

[15] Baxter, J. R. *et al.* Reconstruction of the medial talonavicular joint in simulated flatfoot deformity. *Foot & Ankle International* **36**, 424–429 (2015).

[16] Morton, D. J. Evolution of the human foot II. *American Journal of Physical Anthropology* **7**, 1–52 (1924).

[17] Hayafune, N., Hayafune, Y. & Jacob, H. Pressure and force distribution characteristics under the normal foot during the push-off phase in gait. *The foot* **9**, 88–92 (1999).

[18] Bennett, M. B., Ker, R. F. & Alexander, R. M. Elastic strain energy storage in the feet of running monkeys. *Journal of Zoology* **217**, 469–475 (1989).

[19] Farris, D. J., Kelly, L. A., Cresswell, A. G. & Lichtwark, G. A. The functional importance of human foot muscles for bipedal locomotion. *Proceedings of the National Academy of Sciences* **116**, 1645–1650 (2019).

[20] Heard-Booth, A. N. *Morphological and functional correlates of variation in the human longitudinal arch*. Ph.D. thesis (2017).

[21] Griffin, N. L., Miller, C. E., Schmitt, D. & D'Août, K. Understanding the evolution of the windlass mechanism of the human foot from comparative anatomy: Insights, obstacles, and future directions. *American Journal of Physical Anthropology* **156**, 1–10 (2015).

[22] Williams, D. S. & McClay, I. S. Measurements used to characterize the foot and the medial longitudinal arch: Reliability and validity. *Physical Therapy* **80**, 864–871 (2000).

[23] Leakey, M. D. & Hay, R. L. Pliocene footprints in the laetolil beds at laetoli, northern tanzania. *Nature* **278**, 317–323 (1979).

[24] Crompton, R. H. *et al.* Human-like external function of the foot, and fully upright gait, confirmed in the 3.66 million year old laetoli hominin footprints by topographic statistics, experimental footprint-formation and computer simulation. *Journal of the Royal Society Interface* **9**, 707–719 (2012).

[25] Harcourt-Smith, W. E. H. *et al.* The foot of Homo naledi. *Nature Communications* **6**, 8432 (2015).

[26] Pontzer, H. *et al.* Locomotor anatomy and biomechanics of the Dmanisi hominins. *Journal of Human Evolution* **58**, 492–504 (2010).

[27] Day, M. H. & Napier, J. R. Fossil Foot Bones. *Nature* **201**, 969–& (1964).

[28] Ward, C. V., Kimbel, W. H. & Johanson, D. C. Complete Fourth Metatarsal and Arches in the Foot of Australopithecus afarensis. *Science* **331**, 750–753 (2011).

[29] Haile-Selassie, Y. *et al.* A new hominin foot from Ethiopia shows multiple Pliocene bipedal adaptations. *Nature* **483**, 565–569 (2012).

[30] Raichlen, D. A., Gordon, A. D., Harcourt-Smith, W. E., Foster, A. D. & Haas Jr, W. R. Laetoli footprints preserve earliest direct evidence of human-like bipedal biomechanics. *PLoS One* **5**, e9769 (2010).

Supplementary information: Available in the online version of the paper.

Acknowledgements: We thank Daniel Lieberman for critical reviews of the entire manuscript. Access to skeletal specimens were provided by Gary Aronsen, Kristof Zyskowski, Eric Sargis, Yale Biological Anthropology Labs and the Yale Peabody Museum. K.J. Meacham III provided experimental support. Soumya James helped with figures. Funding support from the Human Frontier Science Program.

Author contributions: M.V., M.M.B., and S.M. conceived of the study; A.Y. and M.V. designed the foot mimics and A.Y. performed the experiments; C.M.E., A.Y., and M.V. designed, collected and analysed the data from the cadaveric experiments in consultation with S.M.T.; A.Y., C.M.E. and M.V. collected and analysed the morphometric data from cadaveric and living human feet in consultation with A.H.H.; M.A.D. and S.M. performed the mathematical modelling in consultation with M.V.; D.K.S. and M.M.B. performed the shell experiments in consultation with M.V.; M.V. planned and wrote the paper; M.V. planned and prepared the figures and tables; M.V., A.Y., S.M., M.A.D., and M.M.B. wrote the supplement; and all authors contributed to editing the paper.

Author information: The authors have no competing interests.

Online methods

Numerical simulations

We simulated the elastic response of arched shells using the *Shell* interface in the *3D Structural Mechanics* module of COMSOL Multiphysics v5.1 (COMSOL AB, Stockholm, Sweden). The transverse tarsal arch (TTA) is represented by the map for the central plane of the shell given by $\mathbf{S}_\mathrm{T}(x, y) = \left(x, R_\mathrm{T} \sin\theta_y, R_\mathrm{T} \cos\theta_y\right)$ where $\theta_y = y/R_\mathrm{T}$, $x \in \left[-L/2, L/2\right]$, and $y \in \left[-w/2, w/2\right]$ (Fig. E2). For all the simulations, we set $L = 0.1\,\mathrm{m}$ and $w = 0.05\,\mathrm{m}$. The material was modeled as linearly elastic with Young's modulus $E = 3.5\,\mathrm{MPa}$, Poisson's ratio $\nu = 0.49$, and mass density $\rho = 965\,\mathrm{kg/m^3}$.

The boundary at $x = -L/2$ is clamped, i.e. zero displacements and rotations. The conditions at the other boundary $x = L/2$, are a uniform shear load $\mathcal{T}$, zero bending moment along z, and zero in-plane traction so that the displacements are free (see Fig. E2 for axes orientations).

We solve this model for a range of thicknesses t, from 3 mm to 9 mm in steps of 1 mm, and transverse curvature radii $R_\mathrm{T} = 0.03\,\mathrm{m}$, 0.05 m, 0.07 m, 0.1 m, 0.3 m, 5 m, 0.7 m, 1 m and 3 m. For each combination of t and R_T, shear $\mathcal{T}$ ranging from $0\,\mathrm{N/m}$ to $1\,\mathrm{N/m}$ is applied in increments of $0.1\,\mathrm{N/m}$. The resulting out-of-plane displacement δz is measured (Fig. E2(b)), and plotted against $\mathcal{T}$. The slope of these curves extrapolated to $\mathcal{T} = 0$ yield the stiffness defined as $k \equiv w\mathcal{T}/\delta z$.

Continuum shell experiments

We fabricated and measured the stiffness of shells with an arch in the transverse or longitudinal directions, and compared them against a flat plate. These were all fabricated using polymer moulding techniques with PDMS (Poly dimethyl siloxane). The mould was fabricated using additive manufacturing (3D printed using ProJet 460Plus, 3D Systems). The printed mould was few millimeters in thickness, with one side left open. PDMS silicone elastomer (Sylgard 184, Dow Corning) was employed to cast the arch in the mould. Because the volume ratio of the base polymer to the curing agent controls the material bulk modulus for PDMS, the same ratio of 5 parts base polymer to 1 part of curing agent by weight was consistently maintained across all fabricated arches (Supplement S3). During an experiment, the fabricated arch was mounted on the experimental rig with help of clamps that were custom fabricated to exactly match the arch curvature. The clamps were additively manufactured (Stratasys Dimension 1200es) with ABSPlus (Acrylonitrile butadiene styrene) thermoplastic material (glass transition temperature 108°C). One end of the clamped arch was affixed to a rigid frame, and the other end of the clamped arch was pushed upon by a thin edge ("knife-edge") that was mounted on a force sensor attached to a vertical translation stage (Fig. E3a). The forces were measured using a data acquisition system (LabView, National Instruments) at 2 KHz for 1 second duration. The load test was performed under quasi-static loading of the arch sample by providing small displacements (quasi-static steps) of 5×10^{-5} m (50 μm) per step for a total of 10 quasi-static steps (5×10^{-4} m or 500 μm). Forces were measured after each quasi-static displacement. The slope of the force-displacement curve is the stiffness K for the arch sample. Three experimental runs were conducted for each arch and their force-displacement curves were reproducible to within measurement error.

Foot mimics

We designed, fabricated and performed load-displacement tests on mechanical mimics of the foot that were transversally curved (Fig. 2, Fig. E4, Supplement S4). The mimic was comprised of three rigid metatarsals hinged at their bases. Instead of every bone in the foot, the mimics were simplifications that captured the longitudinal bending of the metatarsals and lumped all midfoot mobility into hinges at the proximal base of the metatarsals.

The metatarsals were of length L and the hinges were arranged in a transverse arch of curvature c so that the axis of each hinge was at an angle with its neighbour (Fig. 2c, Fig. E4a). Each hinge had an extension spring held at a fixed moment arm equal to half the thickness t and provided torsional stiffness (Fig. E4b). An inter-metatarsal transversally oriented spring connected adjacent metatarsals at the distal end and would resist any splaying induced by the transverse arch.

In hominin feet, the distal end of the metatarsals are level on the ground when loaded. Therefore,

presence of a TTA implies increasing torsion for the lateral metatarsals (Fig. E6b,c). The distal end of the metatarsals in the mimics were made to rest on horizontal, low-friction metallic platforms (Fig. E4a). The vertically staggered arrangement of the platforms mimics the effect of the distal end of the metatarsals being on the same horizontal level. The platforms were attached to a micrometer-precision translation stage for applying vertical displacements. The base of the hinge was rigidly clamped to a six-axis force sensor (JR3 Inc., CA, USA) to measure the reaction forces due to the displacement. Stiffness was estimated as the slope of the force-displacement curve in each trial.

Multiple geometries of the foot were tested and the dimensions chosen to approximate the metatarsal lengths and midfoot widths of hominin feet, including chimpanzees and humans. The length L was varied from 75–125 mm (3 values), thickness t from 18.5–26.8 mm (3 values), and curvature from 0–0.025 mm^{-1} (6 values). The spring constants, measured in an Instron materials testing machine, were 1.76 N/mm and 0.70 N/mm for the longitudinal and transverse springs, respectively. Three trials were performed for each foot and the force-displacement data were reproducible to within measurement error.

The normalized stiffness is $\hat{K} = K/K_{\mathrm{flat}}$. For a flat mimic of length L, thickness t and longitudinal spring stiffness k_ℓ per unit-width, the longitudinal stiffness is given by $K_{\mathrm{flat}} = 3k_m(t/2)^2/L^2$ (Supplement S4.3). In a general setting, the longitudinal spring stiffness would be proportional to the width w of the midfoot by virtue of accommodating a greater amount of parallel elastic tissues. Therefore, the longitudinal stiffness is parametrised by the stiffness per unit-width $k_\ell = 3k_m/w$.

The equation S4.4 for the stiffness of a flat mimic was independently verified using load-displacement tests of 8 different flat mimics (Fig. E4c, Supplement S4.4). We use this relationship to normalize the measured stiffness of all the mimics by a single chimpanzee-like flat mimic of length $L_0 = 75$mm, thickness $t_0 = 18.5$mm, width $w_0 = 60$mm, and whose measured stiffness is K_0. By definition, the normalized stiffness of the chimpanzee-like flat mimic is $\hat{K}_0 = 1$. Therefore, the measured stiffness K of a mimic with length L and thickness t is normalized according to,

$$\hat{K} = \frac{K}{K_0}\left(\frac{L}{L_0}\right)^2\left(\frac{t_0}{t}\right)^2\left(\frac{w_0}{w}\right). \tag{M1}$$

Cadaveric feet

We conducted three-point bending tests using a materials testing system (Instron model 8874) on two fresh frozen cadaveric feet obtained from posthumous female donors (age: 55, 64 years, body weight: 1021 N and 595 N). The loading protocol and boundary conditions under the foot followed Ker et. al[9]. The tibia and fibula were transected midshaft and implanted in Bondo Fiberglass Resin (3M) and secured to the displacement-controlled force sensor on the Instron actuator. The ankle was at a neutral angle of 90°. The heel rested on a rigid platform that was mounted on low-friction sliders to permit foot length changes. The forefoot rested on a highly lubricated surface to permit the foot to naturally deform in all directions when loaded. The contact point on the heel was maintained at the posterior end by placing the heel at the anterior edge of the sliding heel plate so that the heel force mimics the action of the Achilles tendon. The tests were quasi-static with a displacement rate of 0.5 mm/s to 0.6 mm/s.

The displacement required to achieve a load of 3× body weight was measured and then cyclically applied 10–15 times. The last cycle was used for analyses because there was some stress relaxation during the first 6–7 cycles. The area under the force-displacement curve is the work W needed to deform the foot. Following equation (S5.4) W yields an effective stiffness of the foot K_{eff} given by

$$K_{\mathrm{eff}} = \frac{2}{z_{\mathrm{peak}}^2}\int_0^{z_{\mathrm{peak}}} F\,dz. \tag{M2}$$

The same measurements were repeated after bisecting the distal transverse metatarsal ligaments, the skin between the toes, and the muscles and fascia connecting the metatarsals. The inter-metatarsal tissues were transected from the dorsal surface of the foot and the depth of the cut was restricted extend no deeper

than the plantar plane of the metatarsal shafts. So, none of the branches of the plantar fascia or other midfoot ligaments were affected.

Because the applied displacement was the same for the intact feet and those with bisected intermetatarsal tissues, the ratio of work is equal to the ratio of the effective stiffness (equation S5.5).

Monte Carlo simulations

Anatomical variability in the size of feet (Table E2) is incorporated using Monte Carlo simulations to generate statistics for normalized curvature (Fig. 4). The histograms generated from the Monte Carlo simulations are mostly non-Gaussian. Therefore, the median and quartiles are reported in addition to the mean and standard deviation (SD). We used 1 million random combinations of the anatomical dimensions, where each dimension was drawn from an independent Gaussian distribution with means and standard deviations according to Tables E2 and E3. Increasing the size of the Monte Carlo beyond a million samples had no effect on the statistics of the estimated quantities, for the number of significant digits reported. The Monte Carlo simulations likely overestimate the variance of relevant ratios such as w/L and t/L in comparison to hominin feet, because we use independent variation of all dimensions and do not incorporate covariation that may exist. Such inflation of variance because of an assumption of independence of variables is evident in comparing primary measurements versus Monte Carlo estimation of $\hat{c}$ for humans (Table E2).

Morphometrics of feet of extant species

Humans: Human morphometrics were obtained from 12 individuals (6 cadaveric, 6 human volunteers) using radiographic computed tomography (CT X-ray imaging) and software-based segmentation and 3D model reconstruction.[31,32] These feet were all evaluated by a clinical radiologist and identified as non-pathological. The collection, analyses and reporting of live human subjects' data were approved by the Yale IRB. Details on the subjects and CT data processing methods are in the Supplement S5.1

We measured the lever length L following the standard definition as the distance from the posterior end of the calcaneus to the anterior end of the third metatarsal's distal head. The width w is measured at the tarsometatarsal joint, as the mediolateral separation of the most medial aspect of the distal articular surface of the medial cuneiform to the most lateral aspect of the distal articular surface of the cuboid. The thickness t is defined as the dorso-plantar thickness of the proximal head of the third metatarsal, or the average of the second and fourth, when the third metatarsal data are unavailable. The curvature c is based on the torsion θ_{MT4} of the fourth metatarsal, which was measured using the shape of the articular surface using established protocols.[26].

Non-human primates: Published data were used for morphometrics analysis of non-human primates: *Pan troglodytes* (total n=106),[26,28,29,33–35] *Gorilla gorilla* (total n=59),[26,28,29,33,35], *Chlorocebus aethiops* (total n=56),[33,36] and *Macaca nemestrina* (total n=44).[33,37,38]

Published data are sparse and not all necessary measurements were available for a single sample in the published literature on *C. aethiops* and *M. nemestrina*. Therefore, we added data from specimens that were most similar in their lever length L to the mean value reported in the literature. We carried out these measurements using software-based photogrammetry[39] of high resolution images, and cross-verified with measurements using a digital caliper (0.01 mm resolution). The *C. aethiops* foot is from the Yale Biological Anthropology Laboratory (YBL.3032a) and the *M. nemestrina* specimen from the Yale Peabody Museum (YPM MAM 9621).

Mean and standard deviation (SD) of the lever length L were estimated from published data for the chimpanzee,[33–35] gorilla,[33,35], *C. aethiops*,[33,36] and *M. nemestrina*.[33,37,40] Mean w is estimated from reported w/L or dorsal skeletal views for chimpanzees and gorillas,[33,34], and primary measurements for *C. aethiops* and *M. nemestrina*. To estimate the SD of w, we used reported variability in the mediolateral width of the proximal metatarsal heads for all species[26,28,29] to estimate the coefficient of variation (SD/mean), and applied that to w. The mean and SD of t were all obtained from published values,[28,29] and confirmed with primary measurements for available specimens. Torsion of the fourth metatarsal θ_{MT4} is used to estimate the transverse curvature, and published values were used for all non-human

species included in this study[25,26,28,29]. For species where the feet are regarded as flat, we used the same metatarsal torsion values as *P. troglodytes*.

Fossil feet

We used photogrammetry[39] on published images of fossil feet (Fig. 4d), and also data tables that accompanied the publication of these fossil data to estimate necessary dimensions and ratios.[25–29]

Among the fossil feet, all but the foot of *Homo naledi*[25] were incomplete in some regard. For those incomplete feet, an extant species was selected as a template by taking into consideration published analyses of other postcranial and cranial elements. Based on this, *Homo sapiens* was chosen as the template for *Homo erectus* (Dmanisi)[26] and *Homo habilis* (Olduvai hominin),[27] and *Gorilla gorilla* was chosen as the template for *Australopithecus afarensis* (AL 333)[28] and the unknown hominin foot found in Burtele.[29] For example, the sole fourth metatarsal of the *A. afarensis* does not permit the direct estimation of w. However, only the ratio w/L is necessary for the analyses, and the ratio for the gorilla is used for the Monte Carlo analysis of the fossil. The metatarsal however provides a direct measurement of t, but not of L. Therefore, to estimate the ratio t/L, we incorporate the measured thickness t and the gorilla's ratio t_g/L_g by using the formula,

$$\frac{t}{L} = \frac{t}{\langle t_g \rangle} \frac{t_g}{L_g}, \tag{M3}$$

where $\langle t_g \rangle$ is the mean t for the gorilla. This template-based estimation therefore incorporates direct measurements where available, without assuming that the fossil exactly resembles the extant template.

Curvature of hominin feet from metatarsal torsion

Following standard practice in the literature[26,28], we use the torsion of the fourth metatarsal (θ_{MT4}) to estimate TTA curvature. This measure also facilitates the estimation of TTA curvature using partial or disarticulated fossils. When the proximal metatarsal heads form a transverse arch and the distal metatarsal heads rest on the ground, the lateral metatarsals increasingly acquire torsion about their long axis (Fig. 4b, E6b,c). We compared the torsion-based estimate of curvature versus using the external geometry of the dorsal surface of the skeleton and found good correspondence (Supplement S5.1, Fig. E6d). The torsion θ_{MT4} arises from the curvature c over the width w of the tarso-metatarsal articulation, and therefore the curvature is approximated by $c = \theta_{\mathrm{MT4}}/w$. Using equation (1), the torsion-based estimate of the normalized curvature parameter for the TTA is,

$$\hat{c} = \frac{\theta_{\mathrm{MT4}}}{(w/L)\,(t/L)}. \tag{M4}$$

Additional references for online methods

[31] Fedorov, A. *et al.* 3d slicer as an image computing platform for the quantitative imaging network. *Magn Reson Imaging* **30**, 1323–41 (2012).

[32] Yushkevich, P. A., Gao, Y. & Gerig, G. Itk-snap: An interactive tool for semi-automatic segmentation of multi-modality biomedical images. In *2016 38th Annual International Conference of the IEEE Engineering in Medicine and Biology Society (EMBC)*, 3342–3345 (IEEE, 2016).

[33] Schultz, A. H. Relations between the lengths of the main parts of the foot skeleton in primates. *Folia Primatologica* **1**, 150–171 (1963).

[34] Gomberg, D. N. Form and function of the hominoid foot (1981).

[35] Wang, W. J. & Crompton, R. H. Analysis of the human and ape foot during bipedal standing with implications for the evolution of the foot. *Journal of Biomechanics* **37**, 1831–1836 (2004).

[36] Anapol, F., Turner, T. R., Mott, C. S. & Jolly, C. J. Comparative postcranial body shape and locomotion in chlorocebus aethiops and cercopithecus mitis. *American Journal of Physical Anthropology* **127**, 231–9 (2005).

[37] Sirianni, J. E., Swindler, D. R. & Tarrant, L. H. Somatometry of newborn macaca nemestrina. *Folia Primatologica* **24**, 16–23 (1975).

[38] Rodman, P. Skeletal differentiation of macaca fascicularis and macaca nemestrina in relation to arboreal and terrestrial quadrupedalism. *Am J Phys Anthropol* **51**, 51–62 (1979).

[39] Schindelin, J. *et al.* Fiji: an open-source platform for biological-image analysis. *Nature Methods* **9**, 676–82 (2012).

[40] Hamada, Y. Standard growth patterns and variations in growth patterns of the japanese monkeys (macaca fuscata) based on an analysis by the spline function method. *Anthropological Science* **102**, 57–76 (1994).

Extended data figures and tables

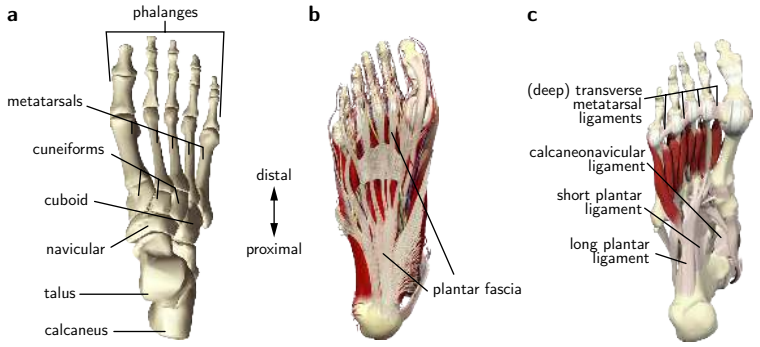

Figure E1. Illustrated anatomy of the foot. a, Identification of the bones of the foot that are referred to in the main text. The cuneiforms, cuboid and the navicular are collectively referred to as the tarsal bones. **b,** The plantar fascia, a tough elastic band, extends from the calcaneus to the distal end of the phalanges. The fascia split and rejoin at multiple locations. **c,** The long plantar, short plantar and calcaneonavicular ligaments are located in the midfoot and are primarily longitudinally oriented. The deep and superficial transverse metatarsal ligaments are examples of stiff, transversally oriented elastic tissues between the metatarsals. Anatomical images from Primal Pictures.

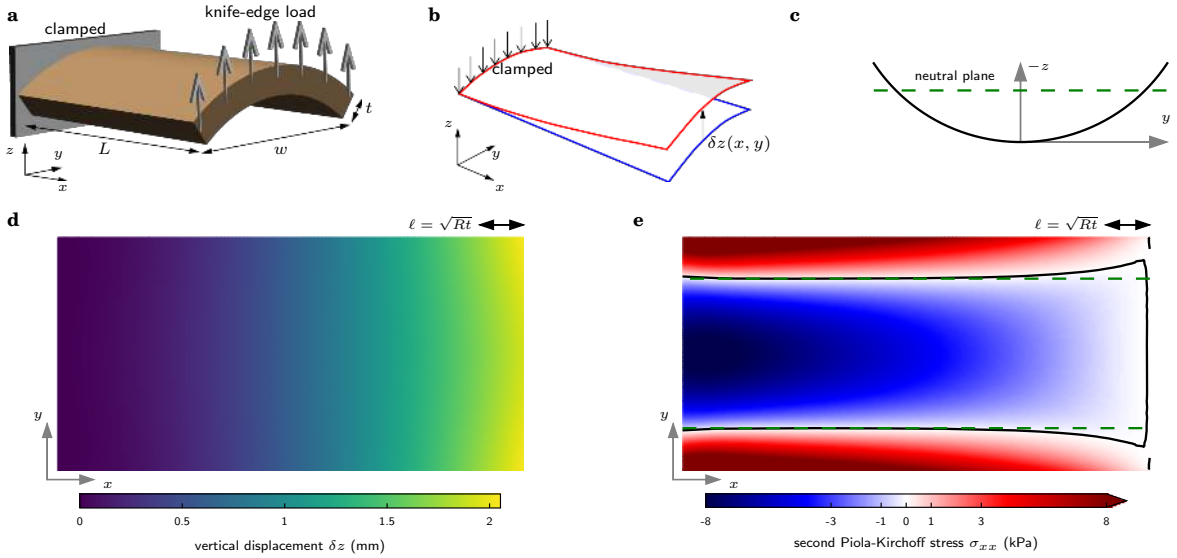

Figure E2. Mathematical and computational analysis of continuum elastic shells. a, The shell is clamped at one end, and loaded with a knife-edge at the other. It is of length L, width w, thickness t, and has radius of curvature R (curvature $c = 1/R$). **b,** The free end displaces by a height δz upon loading, and reaction forces at the clamped end resist deformation. **c,** A cross-sectional view of the shell shows the location of the neutral plane, if the shell were to act as an elastic beam. **d,** Out-of-plane (z-axis) displacement profile for one numerical simulation of a shell ($L = 0.1$ m, $w = 0.05$ m, $t = 0.003$ m, $R = 0.03$ m). Most of the displacement happens close to the loaded edge, unlike an elastic beam. **e,** The stress component σ_{xx} is shown as a color-map of the undeformed shell. In an elastic beam, the intersection of the neutral plane with the shell (panel c) would exactly match the locations of zero stress. Because of curvature-induced in-plane stretching, the zero stress curve differs from the neutral plane predictions in the vicinity of the loaded edge, and to a lesser extent, near the clamped boundary.

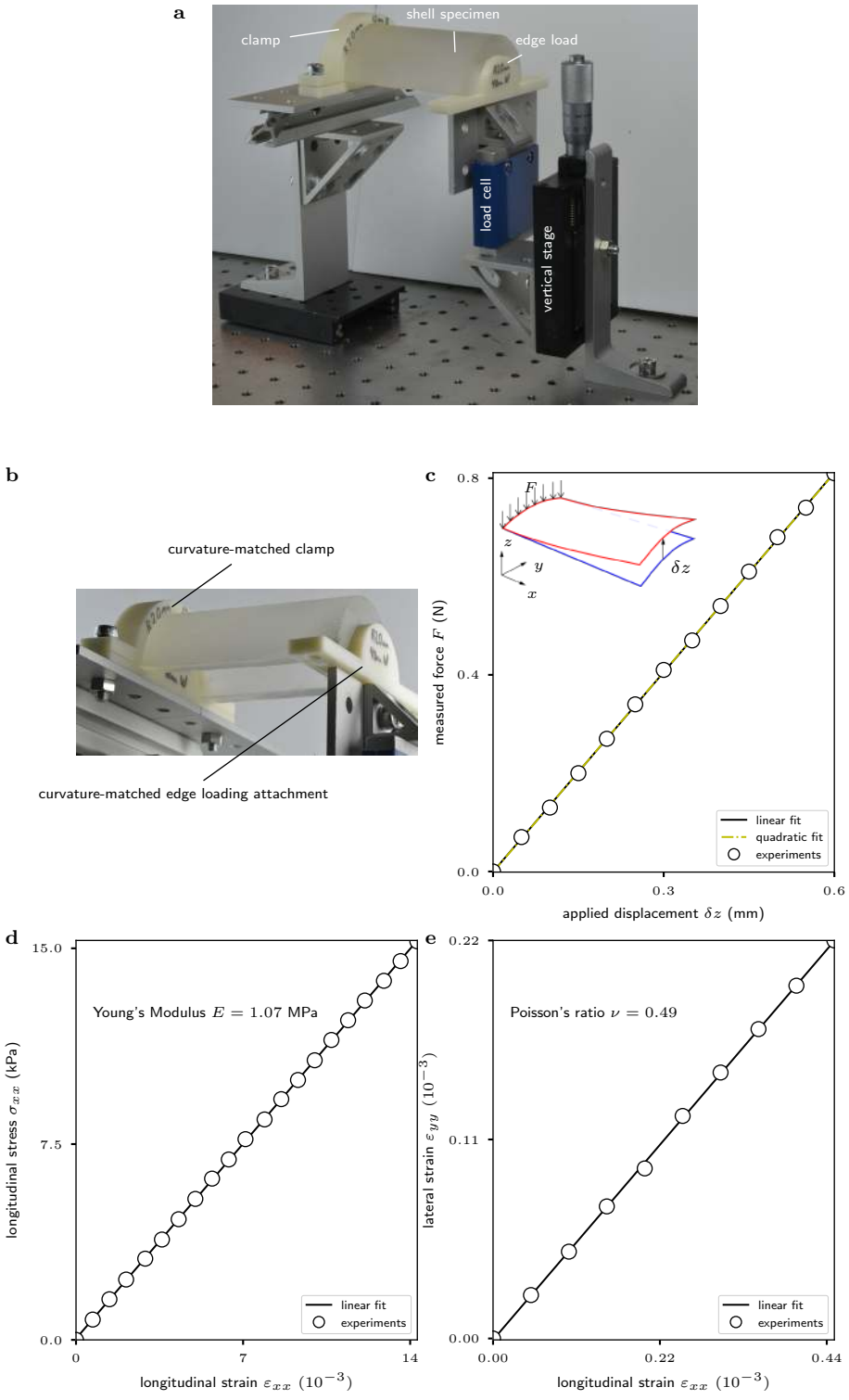

Figure E3. Experimental characterization of arched shells. a, The experimental setup used in stiffness measurements. **b,** A close-up of the shell from underneath shows how a curvature-matched edge loading attachment was used to mimic a theoretical "knife-edge". A curvature-matched clamp was fixed and glued to the other end of the shell. **c,** Representative data that show the linearity of the force-displacement data. The best fit quadratic is indistinguishable from the linear fit to within sensor resolution. **d,** The Young's modulus and **e,** Poisson's ratio of the PDMS material used in fabricating the shells were estimated from simultaneous stress and strain measurements during an extension test of a rectangular PDMS block.

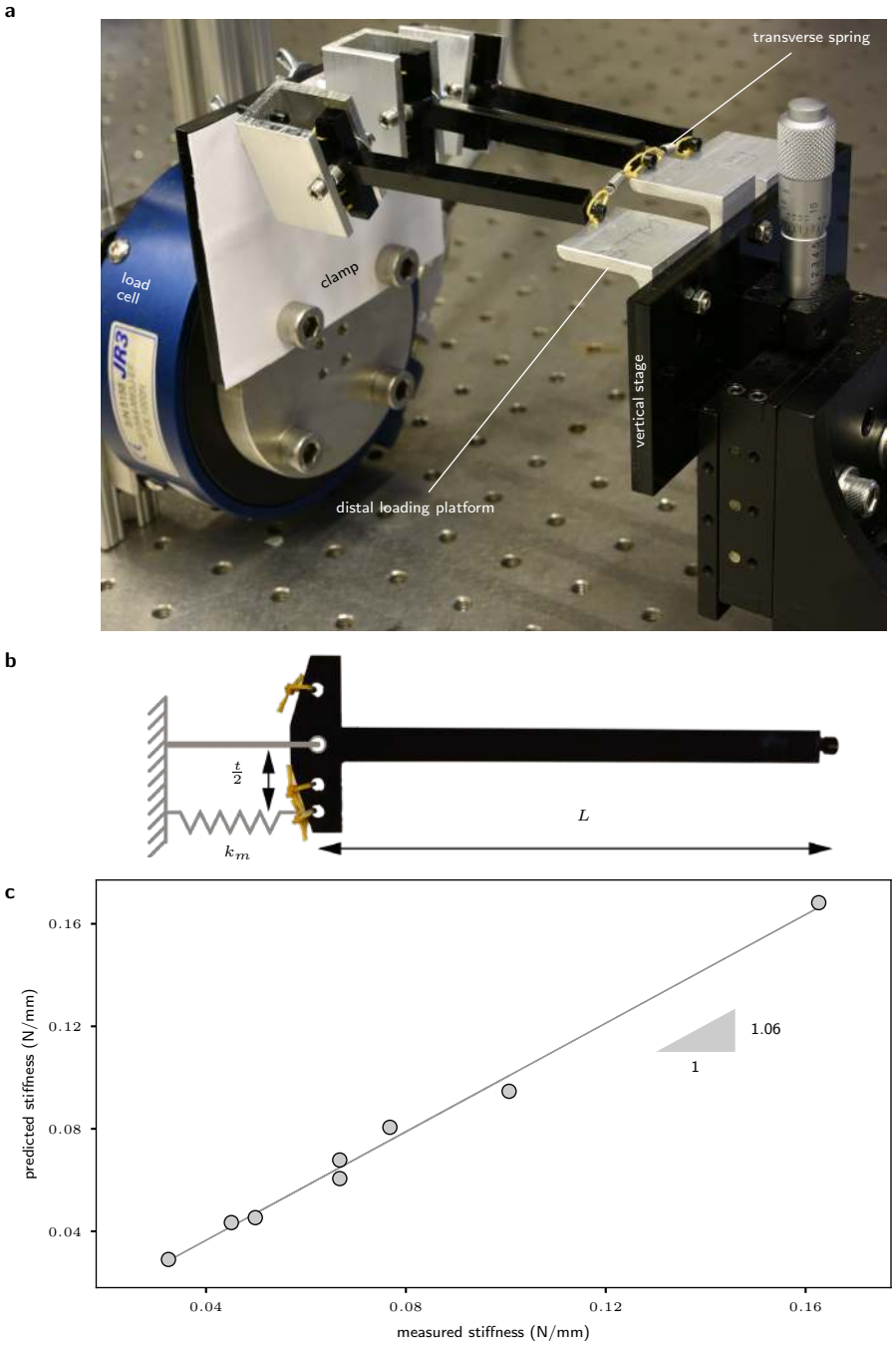

Figure E4. Design and characterization of discrete mechanical foot-mimics. a, Experimental arrangement for load-displacement measurements. The distal loading platforms for the three metatarsals are staggered in height so that all three metatarsals are loaded vertically despite the transverse curvature. In hominin feet, this is accomplished by the metatarsal torsion. **b,** Side view of a single metatarsal showing the length L and thickness t for the foot mimics. The effect of thickness is to provide a moment arm for the longitudinal spring and thereby affect the rotational stiffness of the hinge. **c,** Mimics of three different thickness were fabricated and the thickness was estimated using load-displacement measurements on curvature-free flat mimics. The accuracy of the estimated thickness values are evaluated by plotting the predicted stiffness based on the thickness estimates versus the measured stiffness. Details of the thickness estimation technique and statistics of the stiffness-stiffness correlation are provided in Supplement S4.4.

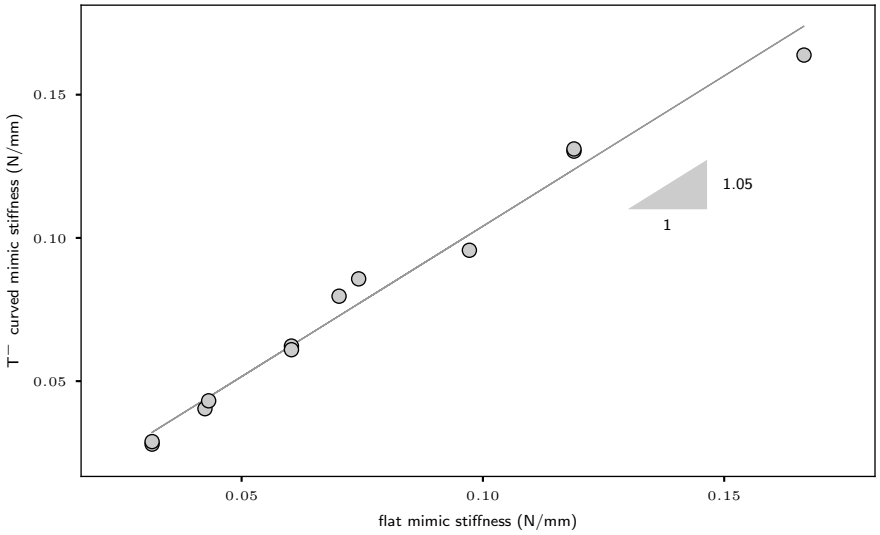

Figure E5. Effect of cutting the transverse springs in mechanical foot-mimics. Stiffness of transversally curved foot mimics lacking the transverse inter-metatarsal springs (T^-) is strongly correlated with the stiffness of flat mimics with intact transverse inter-metatarsal springs.

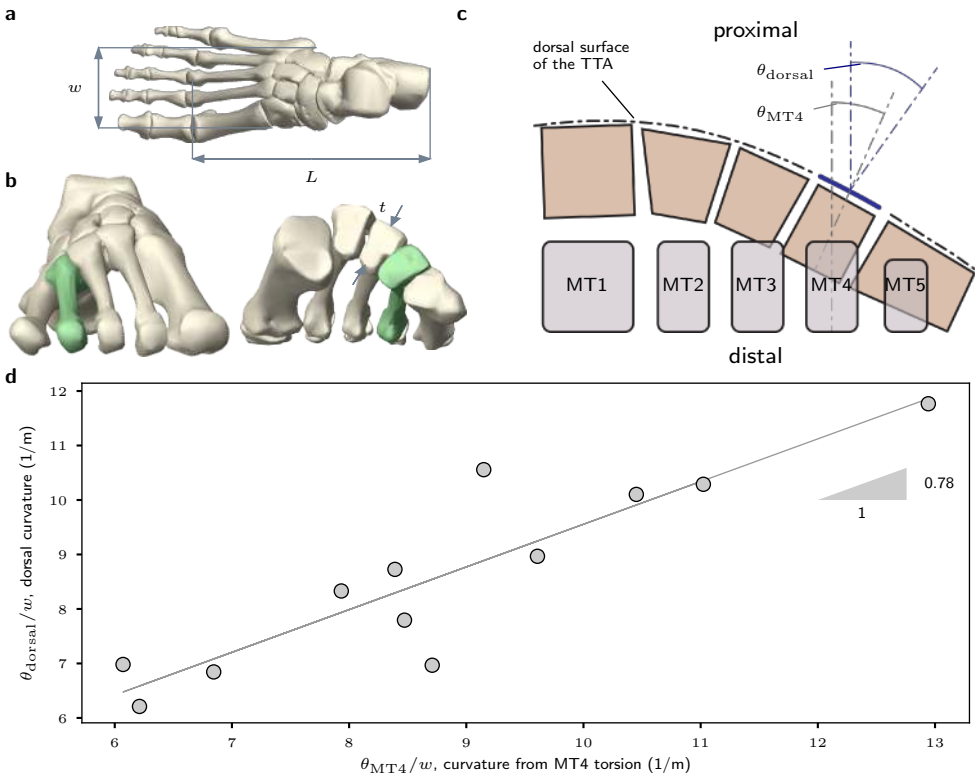

Figure E6. Transverse curvature of biological feet. a, b, Definitions of the length L, width w, and thickness t. The fourth metatarsal is highlighted in green. **b, c,** The distal heads of the metatarsals rest flat on the ground and the proximal heads are raised away from the ground to varying degrees because of the TTA. As a result, the lateral metatarsals accrue torsion about their long axis. **c,** The curvature of the TTA was estimated using the torsion of the fourth metatarsal θ_{MT4}. In addition, the average curvature was also estimated using the angle of the normal to the dorsal surface of the fourth metatarsal θ_{dorsal}, as measured in the midfoot (equation S5.3). **d,** Linear regression of the two different method to estimate TTA curvature. Details of curvature estimation procedure and statistical results of the regression are provided in Supplement S5.1.

Table E1. Table of estimated stiffness values from cadaveric stiffness measurements and from published load versus displacement data for humans[9], *C. aethiops* and *M. nemestrina*.[18] In addition to stiffness of the intact human foot (K_h), the cadaveric experiments performed in the present study included transection of the transverse inter-metatarsal elastic tissues, shown as $K_{\mathrm{T}-}$. The published data for the three species include intact feet (K_h, K_m and K_c) and feet with transection of the plantar fascia ($K_{\square,\mathrm{pf}-}$), the long plantar ligament ($K_{\square,\mathrm{lp}-}$), the short plantar ligament ($K_{\square,\mathrm{sp}-}$) and the calcaneonavicular ligament ($K_{\square,\mathrm{cn}-}$). These estimates were obtained by digitizing the published plots[9,18] of load versus displacement (using B. Tummers, DataThief III. 2006). The contribution of each of the transected tissues are represented as the ratio of the loss in stiffness after transection to the intact stiffness of the same foot. The transections by Ker et al.[9] and Bennett et al.[18] were performed in the same sequence as listed in this table. This shows the significant role played by the transverse elastic tissues and plantar fascia in human feet. Also evident is the similar role of the long plantar and short plantar ligaments in human and monkey feet.

Species	Foot condition	Variable	Estimated value
		Cadaveric data collected for this study	
Homo sapiens	intact	K_h (N/mm)	324; 278
	−transverse tissue	$K_{\mathrm{T}-}$(N/mm)	189; 149
		$(K_h - K_{\mathrm{T}-})/K_h$	42%; 46%
		Previously published[9,18] cadaveric data	
Homo sapiens	intact	K_h (N/mm)	481
	−plantar fascia	$K_{h,\mathrm{pf}-}$ (N/mm)	369
		$(K_h - K_{h,\mathrm{pf}-})/K_h$	23%
	−long plantar ligament	$K_{h,\mathrm{lp}-}$ (N/mm)	241
		$(K_{h,\mathrm{pf}-} - K_{h,\mathrm{lp}-})/K_h$	27%
	−short plantar ligament	$K_{h,\mathrm{sp}-}$ (N/mm)	102
		$(K_{h,\mathrm{lp}-} - K_{h,\mathrm{sp}-})/K_h$	29%
	−calcaneonavicular ligament	$K_{h,\mathrm{cn}-}$ (N/mm)	61
		$(K_{h,\mathrm{sp}-} - K_{h,\mathrm{cn}-})/K_h$	9%
Macaca nemestrina	intact	K_m (N/mm)	177
	plantar fascia removed	$K_{m,\mathrm{pf}-}$ (N/mm)	170
		$(K_m - K_{m,\mathrm{pf}-})/K_m$	4%
	−long plantar ligament	$K_{m,\mathrm{lp}-}$ (N/mm)	117
		$(K_{m,\mathrm{pf}-} - K_{m,\mathrm{lp}-})/K_m$	30%
	−calcaneonavicular ligament	$K_{m,\mathrm{cn}-}$ (N/mm)	85
		$(K_{m,\mathrm{lp}-} - K_{m,\mathrm{cn}-})/K_m$	18%
Chlorocebus aethiops	intact	K_c (N/mm)	132

Table E2. Foot morphometrics for extant species from primary data for humans and Monte Carlo estimates for all species. For the Monte Carlo estimation, the dimensions are modelled as Gaussian random variables. Mean values and standard deviations were obtained from reported values in the literature (Online methods, sub-section *Morphometrics of feet of extant species*, for details). Although the primary data were smaller feet than the published data, the ratios w/L and t/L were nearly equal. The morphometric variables are the lever-length of the foot L, width of the tarso-metatarsal articular region w, dorso-plantar thickness of the third metatarsal t, and torsion of the fourth metatarsal θ_{MT4}. From these, the normalized curvature parameter $\hat{c}$ was estimated.

Species	L (mm)		w (mm)		t (mm)		θ_{MT4} (deg)		$\hat{c}$	
	mean	SD	mean	SD	mean	SD	mean	SD	mean	SD
Homo sapiens[a]	177	16.9	50.7	4.0	16.1	1.6	25.0	4.6	16.9	2.7
Homo sapiens[b]	200	14.0	60.0	5.4	18.0	1.6	23.6	7.1	15.6	5.6
Chlorocebus aethiops	85.0	4.3	24.0	1.2	9.0	0.45	0	2.5	0.0	1.5
Macaca nemestrina	100	6.0	35.0	2.1	10.0	0.6	0	2.5	0.0	1.3
Pan troglodytes	130	13.0	52.0	5.2	13.0	1.3	0	2.5	0.0	1.2
Gorilla gorilla	176	17.6	72.5	7.3	16.0	1.6	2.2	1.5	1.1	0.8

[a] Primary data collected by us from 12 samples.
[b] Bootstrapped Monte Carlo analysis using published data.

Table E3. Fossil morphometric data. Values of L, w, t and θ_{MT4} used in estimating the normalized curvature $\hat{c}$ of fossil samples. Variable names with a subscript h refer to human values (e.g. t_h), subscript p to the chimpanzee (e.g. w_p), and subscript g to the gorilla (e.g. L_g). These values are represented by Normal distributions as shown in Table E2. Variables in angled brackets, such as $\langle t_h \rangle$, refer to the mean value shown in Table E2. See online methods for details of source materials.

Species	Specimen	θ_{MT4} (deg)	L (mm)	w (mm)	t (mm)	w/L	t/L
H. naledi	UW 101-1456	38.0	137.0	38.0	16.0	0.277	0.117
H. erectus	D2669, D4165	28.0, 29.0	–	–	17.0	$\frac{w_h}{L_h}$	$\frac{t}{\langle t_h \rangle}\frac{t_h}{L_h}$
H. habilis	OH 8	25.0	112	44.0	–	0.393	$\frac{t_h}{L_h}$
Burtele	BRT VP2/73	26.5	–	–	13.3	$\frac{w_g}{L_g}$	$\frac{t}{\langle t_g \rangle}\frac{t_g}{L_g}$
A. afarensis	AL 333-160	17.0	–	–	17.1	$\frac{w_g}{L_g}$	$\frac{t}{\langle t_g \rangle}\frac{t_g}{L_g}$